RSC Advances

PAPER

Cite this: *RSC Adv.*, 2021, **11**, 35718

Spin filtering controller induced by phase transitions in fluorographane†

Cuicui Sun, ‡[a] Yingjie Jiang,‡*[b] Yanmin Wang, [a] Xiao-Cun Liu, [a] Yanling Wu, [a] Yongling Ding[a] and Guiling Zhang [c]

Received 25th September 2021
Accepted 26th October 2021

DOI: 10.1039/d1ra07161k

rsc.li/rsc-advances

The electronic and transport properties of fluorographane (C_2HF) nanoribbons, *i.e.*, bare (B-C_2HF) and hydrogen-passivated (H-C_2HF) C_2HF nanoribbons, are extensively investigated using first-principles calculations. The results indicate that edge states are present in all the B-C_2HF nanoribbons, which are not allowed in the H-C_2HF nanoribbons regardless of the directions. The spin splitting phenomenon of band structure only appears in the zigzag direction. This behavior mainly originates from the dehydrogenation operation, which leads to sp^2 hybridization at the edge. The H-C_2HF nanoribbons are semiconductors with wide band gaps. However, the band gap of B-C_2HF nanoribbons is significantly reduced. Remarkably, the phase transition can be induced by the changes in the magnetic coupling at the nanoribbon edges. In addition, the B-C_2HF nanoribbons along the zigzag direction show optimal conductivity, which is consistent with the band structures. Furthermore, a perfect spin filtering controller can be achieved by changing the magnetization direction of the edge C atoms. These results may serve as a useful reference for the application of C_2HF nanoribbons in spintronic devices.

1. Introduction

Graphene has garnered significant interest in both scientific research and technological applications due to its unique crystal structure as well as excellent physical, electric, mechanical, and chemical properties.[1] However, the gapless electronic structure and chemical inertness hinders its application in the integration of traditional electronic and optoelectronic devices. To overcome this issue, chemical functionalization has been used to adjust the physical and chemical properties of graphene.[2–4] In particular, significant effort has been devoted to engineer a band gap in graphene by introducing structural defects[5] or by surface functionalization with H or F atoms.[6,7] After covering graphene with heteroatoms, the band gap is opened due to the transformation of sp^2-hybridized carbon into sp^3-hybridized carbon. In contrast to graphene, hydrogenated graphene exhibits fluorescence,[8] paramagnetism,[9] fast heterogeneous electron transfer,[10] and tunable band gap (0–3.7 eV).[11] Fluorographene also shows fluorescence and enhanced electrochemical properties.[12–15] Furthermore, due to the partial similarity between hydrogen and halogen atoms, studies on fluorographane (C_2HF) have been conducted recently.[16–18] The difference in the electronegativity between H and F atoms causes an out-of-plane dipole moment that makes the electronic structure more complex and controllable, which has triggered extensive research enthusiasm.[19–22]

Although several experimental and theoretical studies have focused on the synthesis and properties of fluorographane,[21,23,24] the C_2HF nanoribbons have been hardly investigated.[19] After the formation of one-dimensional (1D) nanoribbons, the electronic and transport properties have been tuned by altering the width, doping hetero atoms, applying external field or strain, edge modification, chemical adsorption, *etc.*[25–27] Among them, edge modification is one of the most popular methods. This is because the basic physical properties of nanoribbons are strongly related with their edge shapes, which may induce the edge states and further result in the spin polarization. Consequently, the effect of various edge passivation states in different nanoribbons has attracted considerable research attention.[28,29] For example, the sp^3 hybridization on the edge atoms of zigzag silicon carbon nanoribbons after the dual-hydrogenation led to a perfect spin filtering behavior (nearly 100% spin filtering efficiency).[30] The edge dehydrogenation caused a transition from antiferromagnetic (AFM) state to ferromagnetic (FM) state and effectively improved the spin filtering efficiency.[31] Numerous studies have revealed the influence of edge passivation states on the electronic structure and magnetic properties of nanoribbons. However, the electronic/magnetic properties of the C_2HF nanoribbons with different edge passivation states have not been investigated in

[a]*School of Civil Engineering, Shandong Jiaotong University, Jinan 250300, China*
[b]*State Key Laboratory for Turbulence and Complex System, Department of Mechanics and Engineering Science, College of Engineering, Peking University, Beijing 100871, China. E-mail: yingjiejiang@pku.edu.cn*
[c]*School of Materials Science and Chemical Engineering, Harbin University of Science & Technology, Harbin 150080, China*

† Electronic supplementary information (ESI) available. See DOI: 10.1039/d1ra07161k

‡ Cuicui Sun and Yingjie Jiang contributed equally to this work.

detail. Therefore, in this study, a series of C_2HF nanoribbons with different edge states are investigated to obtain a deeper insight into the quantum behavior of the spin-resolved transport properties. Here, the band structures and transport properties of bare or hydrogen-passivated C_2HF nanoribbons with armchair and zigzag edges are presented. Our results show that the spin filtering can be controlled by changing the magnetization direction of edge C atoms. The effectiveness of this method stems from the fact that it provides an easy and precise control of spin filtering properties. Combining with the advantages of 1D nanoribbons, it is potentially useful for the transfer and treatment of information, allowing faster, low-energy operations in very small and complex devices.

2. Models and calculation methods

The geometrical optimizations were conducted using density functional theory (DFT) implemented in the Vienna *ab initio* simulation package (VASP).[32] The projector augmented wave (PAW) method was used with a cut-off energy of 400 eV. The electronic exchange and correlation energies were described by generalized gradient approximation (GGA) of Perdew–Burke–Ernzerhof (PBE) functional.[33] The atomic positions were relaxed to find the lowest energy configuration with the conjugated gradient method until the force on each atom was smaller than 0.01 eV $Å^{-1}$. To isolate the interaction, a vacuum region of at least 15.0 Å was applied to separate the adjacent nanoribbons. The quantum transport code ATK[34,35] was employed to study the electronic transport properties of the nanoribbons. A kinetic-energy cutoff of 75 hartree was chosen. Further, *k*-point sampling with $1 \times 1 \times 21$ grid was used for the static electronic structure and band structure calculations. A double-ζ plus polarization (DZP) basis set was constructed for the H, C, and F atoms, and the same exchange–correlation functional was adopted. The C_2HF nanoribbons were separated by a 25×35 Å vacuum slab in the $x \times y$-plane to neglect the interactions among the periodic images.

After geometrical optimization, the relaxed structure of C_2HF is a puckered surface, and the perfectly planar graphene plane is locally buckled, as shown in Fig. 1. Here, C_2HF nanoribbons with different edges are considered, including bare and hydrogen-passivated nanoribbons, which are abbreviated as B-C_2HF and H-C_2HF nanoribbons, respectively. The primitive nanoribbons cells with minimum number of atoms marked in Fig. 1 are used in the electronic structure calculations. The lengths of C–C, C–H, and C–F bonds are 1.53, 1.11, and 1.37 Å, respectively. The two-probe models are constructed for the electronic transport simulation, as depicted in Fig. 1. The graphene was selected as the electrode materials of the device along zigzag direction. Since the pristine armchair graphene nanoribbon is a semiconductor, the N-doped armchair graphene nanoribbons[36] are used as electrode materials along the armchair direction. The buffer layers extending from the electrode are used to shield the interaction between the electrodes.

3. Results and discussions

The electronic structures of the B-C_2HF (H-C_2HF) nanoribbons in gas phase are first investigated. It is clear from Fig. 2 and 3 that H-C_2HF nanoribbons have larger band gaps than B-C_2HF nanoribbons, irrespective of zigzag or armchair edges. These larger band gaps indicate that the edge hydrogen-passivated nanoribbons are electrochemically stable with poor charge transport properties. B-C_2HF nanoribbons are extremely different from H-C_2HF nanoribbons. Due to the dehydrogenation operation, the band gap characteristics of B-C_2HF nanoribbons are similar to those of graphene nanoribbons, where the B-C_2HF-zigzag nanoribbon behaves as a conductor and the B-C_2HF-armchair nanoribbon behaves as a semiconductor. Thus, the reduction of the band gap in these nanoribbons can be attributed to the introduction of additional bands. As seen from the Bloch states in Fig. 4, the wave functions of these additional bands (bands I, II, i, and ii), which are called edge-related bands in B-C_2HF nanoribbons, are predominantly localized on the edges. In contrast, the Bloch states of the other bands of C_2HF nanoribbons are distributed at the central region of the nanoribbons, as shown in Tables S1 and S2.† Fundamentally, the dehydrogenation changes the hybridization mode of the edge C atoms from sp^3 to sp^2, and the original strong C–H covalent bonds break into a dangling bond, where the unpaired electrons localized on the edge C atoms increase the activity of the system and reduce the band gap. In addition, these edge-

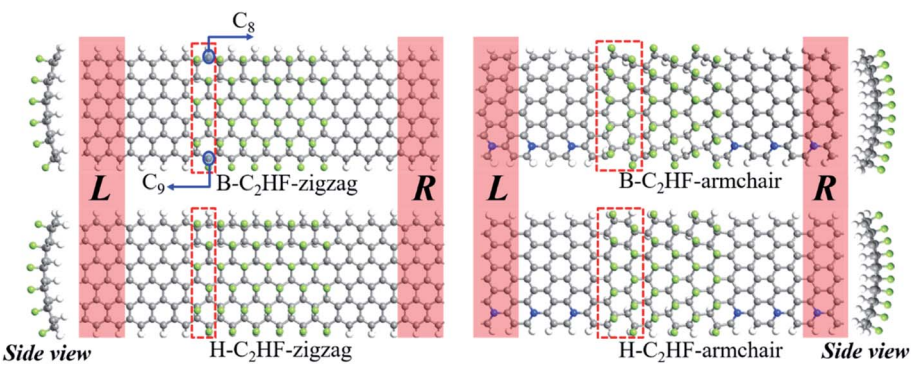

Fig. 1 Two-probe model for the electronic transport simulation of B-C_2HF-zigzag, B-C_2HF-armchair, H-C_2HF-zigzag, and H-C_2HF-armchair. The marked unit nanoribbon cells are selected as the structures for the bulk system calculations.

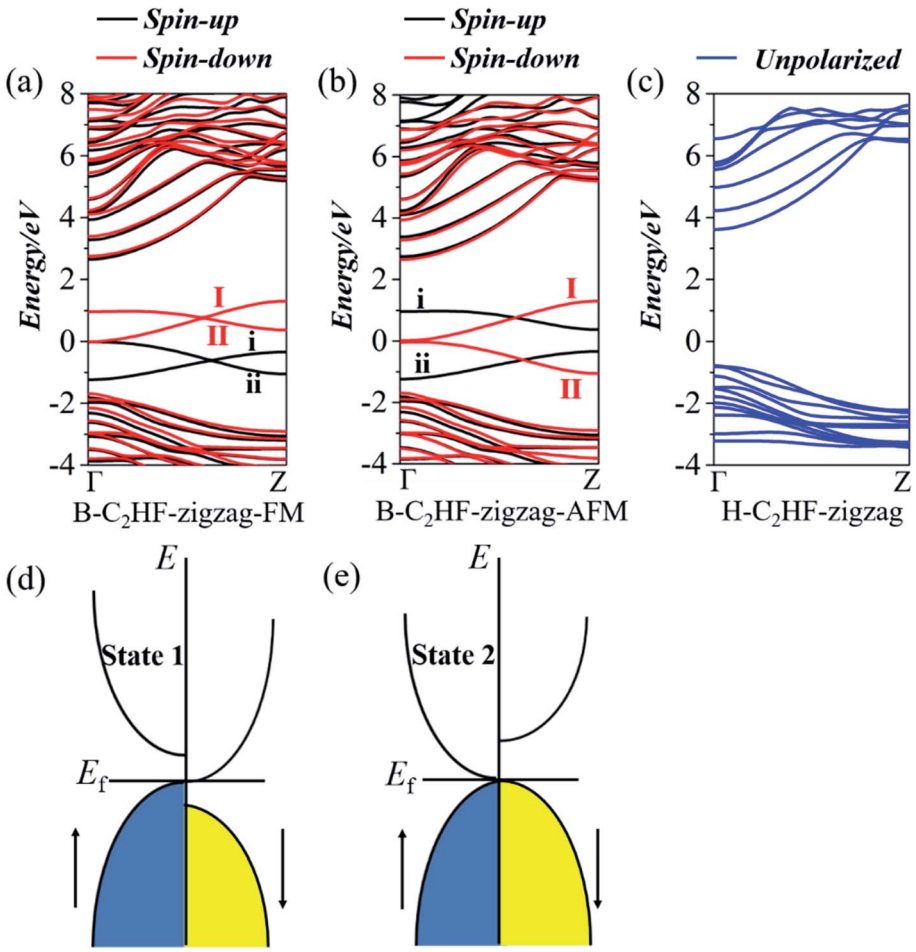

Fig. 2 (a) Band structures of B-C_2HF-zigzag-FM, (b) band structures of B-C_2HF-zigzag-AFM, (c) band structures of H-C_2HF-zigzag nanoribbons, and (d) and (e) energy band diagrams for spin gapless semiconductors of state 1 and state 2.

related bands show excellent dispersion characteristics, and these bands are different from the localized bands caused by impurities[37,38] along the symmetry line of Γ–Z. It can be inferred that the B-C_2HF nanoribbons exhibit excellent charge transport capabilities at low voltages, especially the nanoribbons with zigzag boundaries.

By artificially setting the spin polarizabilities (same or opposite to each other, *i.e.*, FM and AFM state) of the C atoms at the edge of the nanoribbons to simulate an external magnetic field, an interesting phase transition phenomenon is observed in the B-C_2HF-zigzag nanoribbons: a spin gapless

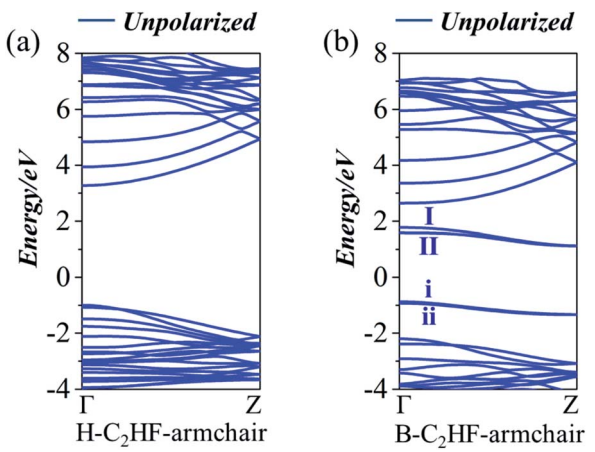

Fig. 3 Band structures of (a) H-C_2HF-armchair nanoribbons, and (b) B-C_2HF-armchair nanoribbons.

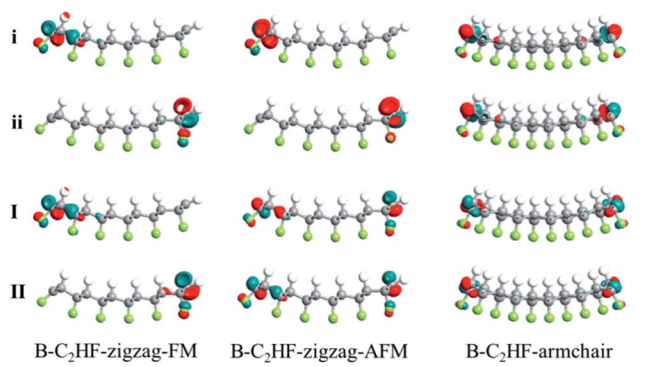

Fig. 4 Bloch states of edge-related bands at Γ for B-C_2HF-zigzag-FM, B-C_2HF-zigzag-AFM, and B-C_2HF-armchair nanoribbons.

semiconductor state 1 to a spin gapless semiconductor state 2. Although, they are all spin gapless semiconductors.[39–41] But, the B-C_2HF-zigzag nanoribbons with the FM state display a spin gapless semiconductor state 1 character: there is a gap between the conduction and valence bands for both the majority and minority electrons, while there is no gap between the majority electrons in the valence band and the minority electrons in the conduction band, as shown in Fig. 2d. However, that with the AFM state behave as a spin gapless semiconductor state 2 character: one spin channel is gapless, while the other spin channel is semiconducting, as shown in Fig. 2e. In other words, the features of the electronic properties can be manipulated by the magnetic field (the variation in the magnetic field indicates the variation in the magnetic coupling mode of the edge C atoms), which means that this transition is experimentally feasible. In addition, another important electronic effect: spin splitting of both AFM and FM states, is shown in Fig. 2. The difference is that both the spin-up and spin-down states show gapless properties in the FM state and the band edge touch at the Fermi level (E_f) at Γ point. However, the charge carriers in the spin-up state are mainly holes, while that in the spin-down state are primarily electrons. Interestingly, the AFM state exhibits different electronic characteristics: the spin-down state presents a gapless character, and it turns into semiconductor with a band gap of 0.72 eV in the spin-up state. The obvious spin splitting near the E_f originates from the change in the electronic configuration of edge C atoms. As mentioned above, the dehydrogenation changes the hybridization state of edge C atoms from sp^3 into sp^2. The unpaired electrons in the adjacent sp^2-hybridized C atoms result in spin splitting. The spin polarization caused by the edge C (C_8 and C_9, as shown in Fig. 1) can also be seen from the magnetic moment in Table S5.† Clearly, the

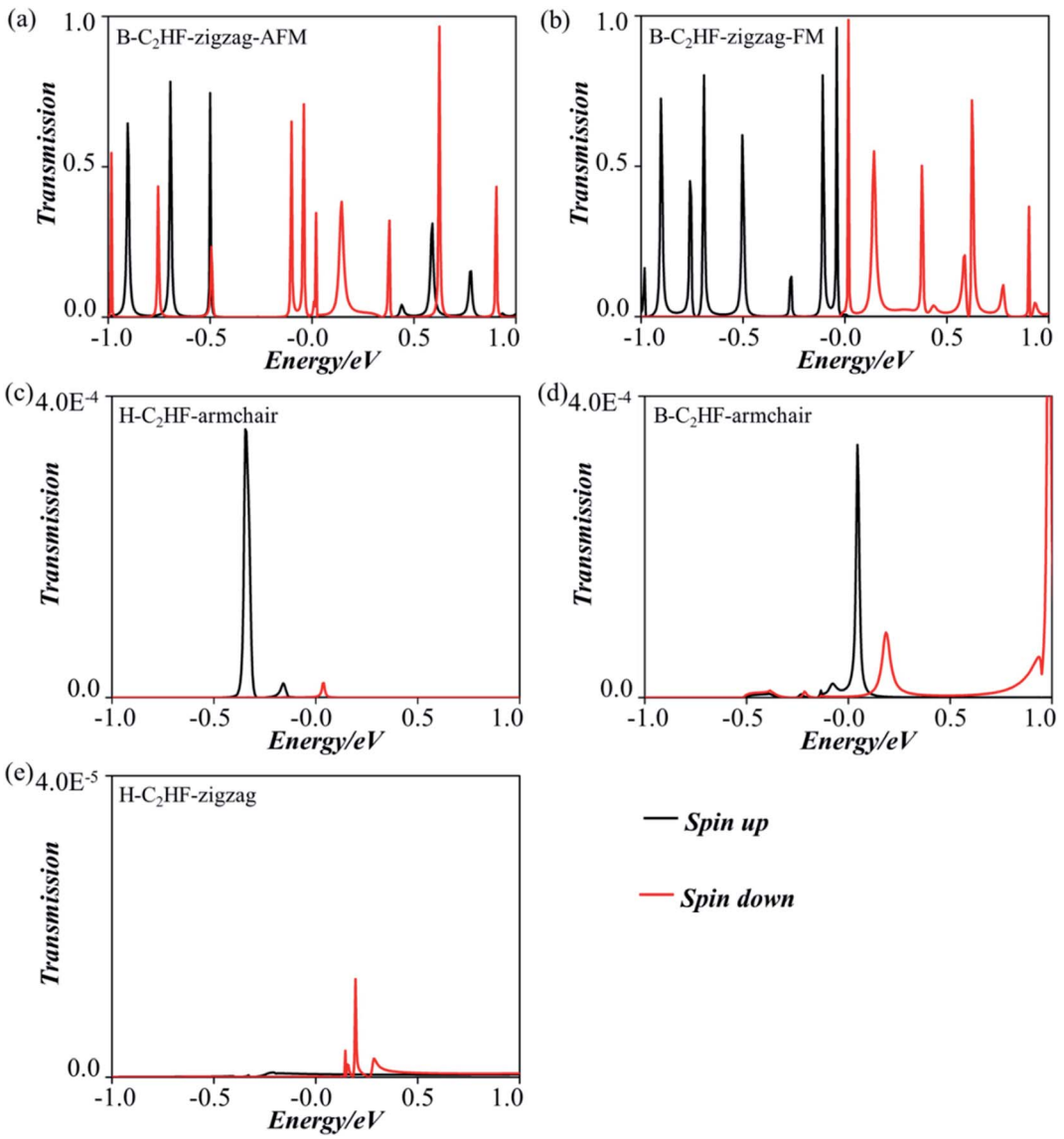

Fig. 5 Transmission spectra of (a) B-C_2HF-zigzag-AFM, (b) B-C_2HF-zigzag-FM, (c) H-C_2HF-armchair, (d) B-C_2HF-armchair, and (e) H-C_2HF-zigzag nanoribbons.

magnetic moment of B-C_2HF-zigzag nanoribbon of both the FM and AFM state mainly arises from the C at the edge. However, a completely different spin splitting is observed in B-C_2HF-armchair nanoribbon. Although such kinds of C atoms are also present in B-C_2HF-armchair nanoribbon, no spin splitting happens due to the different configuration, as shown in Fig. 3b. To determine the reason for this phenomenon, we calculated the Mulliken population of BC_2HF-armchair and B-C_2HF-zigzag nanoribbons. Comparing with the results, it is found that the Mulliken population of the edge C atoms in B-C_2HF-armchair nanoribbons is similar to that in the central region, which has sp^3 hybridization, as seen in Table S3.† In this case, the electrons are paired and no unpaired electron exits. In contrast, the Mulliken population of the edge C atoms in B-C_2HF-zigzag nanoribbons is special: there is almost one charge difference between spin-up and spin-down atoms, indicating the presence of unpaired electrons, as shown in Table S4.†

Another interesting issue is the conductive mechanism of the nanoribbons with various edges. Therefore, the transmission functions were calculated to clarify the quantum behavior and electron transmission channels. We can intuitively find that the most obvious distinction between the five transmission functions is the intensity, which can vary by four or five orders of magnitude or more (Fig. 5). From the analysis of the band structures, it is concluded that all the C_2HF nanoribbons along the armchair direction have a very large band gap. After these nanoribbons are combined with the electrode material, due to the resonance between the electronic wave functions, some energy levels appear near the E_f (as shown in Fig. 6), but these energy levels are highly localized at the interface and cannot promote electron transmission. Consequently, both H-C_2HF-armchair and B-C_2HF-armchair nanoribbons show extremely small transmission coefficients. On the other hand, in the zigzag direction, the hydrogenation of the H-C_2HF-zigzag nanoribbon causes the edge C atoms to become sp^3 hybridized and the electrons are in inert state, causing the energy levels to move away from the E_f. The only few energy levels near E_f in the spin down state of the H-C_2HF-zigzag nanoribbon (Fig. 7c) are also localized in the buffer layers. Correspondingly, the bare nanoribbons B-C_2HF-zigzag show a large transmission value, and it originates from the active single electron in sp^2 hybridization, which introduces more energy levels near E_f, as shown in Fig. 7a and b. Contrary to H-C_2HF-zigzag nanoribbon, these energy levels are all completely delocalized through the scattering region. Of course, this is consistent with the band structures, *i.e.*, B-C_2HF-zigzag nanoribbon shows spin gapless semiconductor character, while H-C_2HF-zigzag nanoribbon shows semiconductor characteristics with a larger band gap. From these results, it can be inferred the conductivity of B-C_2HF-zigzag nanoribbon is optimal. More interestingly, the spin polarization of electrons makes the

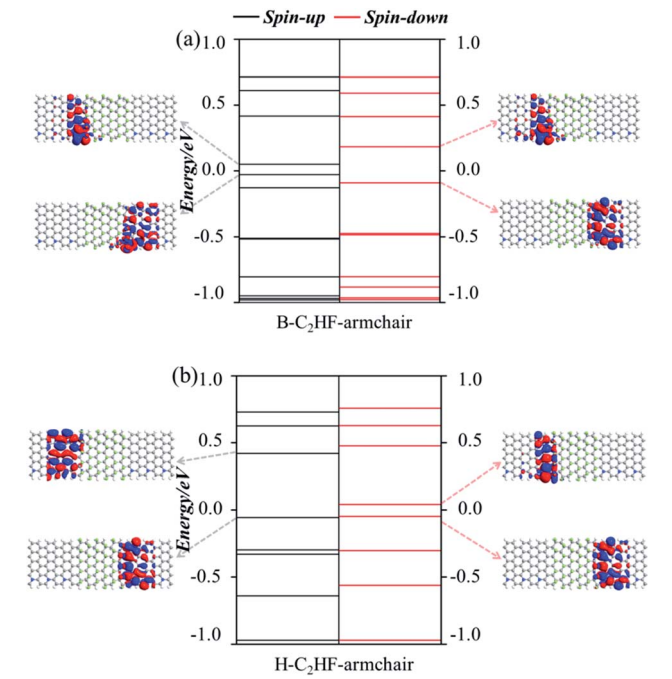

Fig. 6 Molecular energy spectra of (a) B-C_2HF-armchair, and (b) H-C_2HF-armchair nanoribbons.

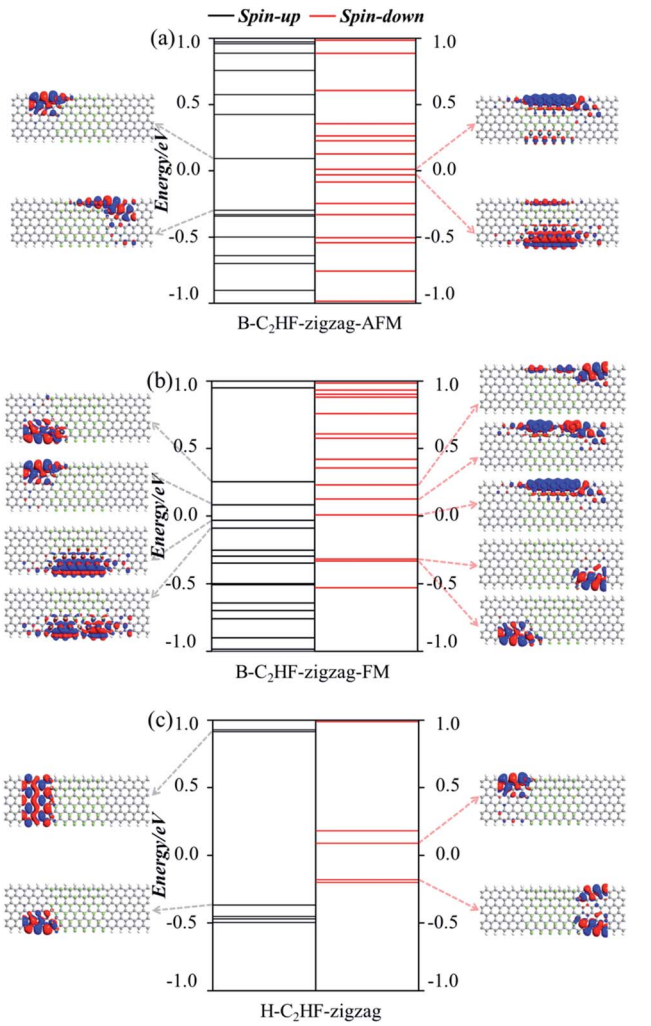

Fig. 7 Molecular energy spectra of (a) B-C_2HF-zigzag-AFM, (b) B-C_2HF-zigzag-FM, and (c) H-C_2HF-zigzag nanoribbons.

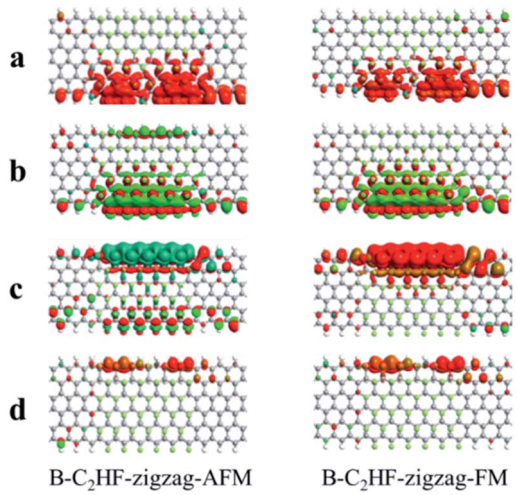

Fig. 8 Transmission energy eigenstates corresponding to the transmission peaks near E_f of B-C_2HF-zigzag nanoribbons.

transport phenomenon more complex. Hereafter, we mainly focus on the spin-related transport of B-C_2HF-zigzag nanoribbons.

Consistent with the band structures, both the AFM and FM states of the B-C_2HF-zigzag nanoribbons are calculated. The conductance of both AFM and FM states is highly spin-polarized. The difference is that the frontier molecular orbitals of the AFM state are dominated almost entirely by the spin-down state, while those of the FM state are equally controlled by spin-up and spin-down states, *i.e.* the highest occupied molecular orbital (HOMO) is provided by the spin-up state, and the lowest unoccupied molecular orbital (LUMO) is dominated by the spin-down state. Specifically, the spin-down electronic state governs the transport in the low voltage range (when the energies of electrons are localized in the range of −0.5 to 0.5 eV) for AFM state, but that is controlled by both spin-up and spin-down for the FM state, which causes the perfect spin filtering, as shown in Fig. 5a and b. The energy level distributions and orbital wave functions in Fig. 7a can provide a deeper perspective to understand this phenomenon: the wave function distributions of frontier orbitals for the two polarization directions are completely different. For the AFM state, these spin-up orbitals are highly localized, but the spin-down orbitals exhibit excellent delocalization. The delocalization may facilitate the construction of effective electron transmission channels. However, for the FM state, taking the E_f as the dividing line, the composition of the electron transmission channels is completely different. The channels with energy above and below the E_f are independently constructed by spin-up and spin-down orbitals, respectively, as shown in Fig. 5b. This is because there are a large number of single electrons with parallel spins in the system. The Hund's rule governs the arrangement of electrons in the orbitals, *i.e.*, each orbital must contain one electron, each spinning in the same direction, before the electrons can be paired in the orbitals. The occupation of single electrons splits the original degenerate spin orbitals, one of which is an occupied spin-up orbital, and the others are empty spin-down orbitals. The partial orbital wave functions intuitively reveal the contribution of related molecular orbitals to the electron transmission. As seen in Fig. 7b, the occupied spin-up orbitals and empty spin-down orbitals display good delocalization characteristics, which can construct effective electron transmission channels.

In addition, the conductance of a device is determined by the spatial distribution of the frontier molecular orbitals.[42] For example, one frontier molecular orbital has a high possibility to resonate with the electronic states in the electrodes if the orbitals spread over the entire device, resulting in a more beneficial conductivity. Therefore, we calculated the eigenstates of the transmission peaks (a, b, c, and d) near the E_f. Obviously, the transmission eigenstates of a, b, c and d, which originate from the edge of nanoribbons, are delocalized across the central region and strongly coupled with two electrodes, as shown in Fig. 8, which is an essential prerequisite for the resonant transmission.

To recapitulate, the edge states play an important role in the transport mechanism. The change in the hybridization of edge C atoms leads to spin splitting. For the FM state, the occupied spin-up orbitals and empty spin-down orbitals can all construct effective electron transmission channels. However, for the AFM state, the spin-down electronic state governs the transport in the low voltage range. Obviously, the spin-up transmission is filtered out during the transition from FM to AFM state. Therefore, we can realize a perfect spin filtering controller through switch the magnetization at any time. This effect can be achieved by changing the magnetization direction of edge C atoms, and the corresponding schematic diagram is shown in

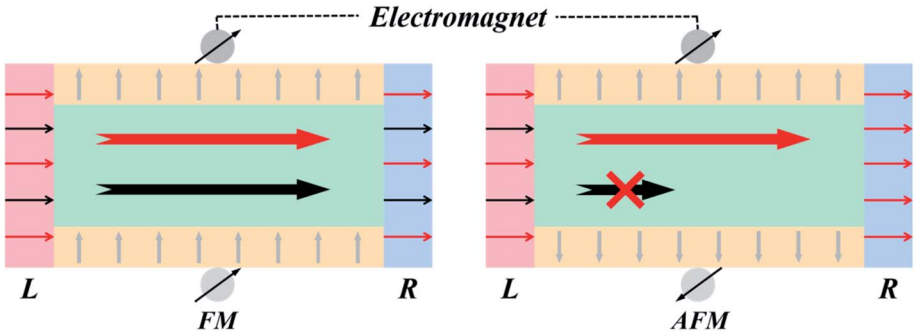

Fig. 9 Schematic diagram of the modulation of system transport properties by external magnetic field.

Fig. 9. Obviously, the frontier molecular orbitals of the FM state are equally controlled by spin-up and spin-down states that lead to two effective electron transmission channels. While for the AFM state, the frontier molecular orbitals are dominated almost entirely by the spin-down state which result in only one effective electron transmission channels. Compared with graphene nanoribbons, the novel B-C_2HF-zigzag nanoribbons exhibit almost perfect spin current switching due to the synergistic effect between the sp^2 and sp^3 hybridization. In the B-C_2HF-zigzag nanoribbons, the sp^3 hybridization mode of the C atoms in the central region causes the system to have a large band gap. On the other hand, the sp^2 hybridization originating from the dehydrogenation of edge C atoms introduces several active bands, which are gapless near E_f. In general, from the perspective of the band structures, the edge-related bands not only exhibit excellent dispersion characteristics similar to graphene nanoribbons, but also display extremely obvious spin splitting. In terms of transport, the spin transmission channels can be easily tuned from on to off state (or *vice versa*) by an external magnetic field under low voltage region.

4. Conclusions

The electronic structure and transmission properties of the C_2HF nanoribbons with different edges were investigated in detail through DFT theoretical calculations. The main difference between B-C_2HF and H-C_2HF nanoribbons was the presence of edge states in the B-C_2HF nanoribbons both along the armchair and zigzag directions. In the armchair direction, the B-C_2HF and H-C_2HF nanoribbons were all semiconductors, and the edge states had a minor effect on the transport properties. In contrast, the edge states improved the conductivity of B-C_2HF-zigzag nanoribbons. The dehydrogenation operation changed the hybridization of edge C atoms from sp^3 into sp^2, resulting in spin splitting. Further, the following electronic feature transition was observed: B-C_2HF-zigzag nanoribbons with FM displayed a spin gapless semiconductor state 1 character, while that with AFM behaved as a spin gapless semiconductor state 2. More interestingly, the spin polarization of electrons caused the transport to become more complex in the B-C_2HF-zigzag nanoribbons. With the transition from FM to AFM state, the system exhibited an obvious spin filtering effect, *i.e.*, the spin-up transmission vanished. Therefore, a perfect spin filtering controller could be realized through the transition between FM and AFM states. Overall, our analysis can serve as practical tool for revealing the nature of the edges in realistic samples and can be used for experimentally exploring the applications of such spin filtering controllers in optoelectronic devices.

Conflicts of interest

There are no conflicts to declare.

Acknowledgements

This work was supported by the Doctoral Scientific Research Foundation of Shandong Jiaotong University (BS50004943), the Scientific Research Fund Project of Shandong Jiaotong University (Z201916 and Z201918), and National Natural Science Foundation of China (51803109 and 51973046).

References

1 K. S. Novoselov, A. K. Geim, S. V. Morozov, D. Jiang, Y. Zhang, S. V. Dubonos, I. V. Grigorieva and A. A. Firsov, *Science*, 2004, **306**, 666–669.
2 F. Obite, *Nanosci. Nanotechnol.*, 2020, **4**, 1–48.
3 N. Chavoshi and R. Jahanmardi, *Fullerenes, Nanotubes, Carbon Nanostruct.*, 2019, **27**, 1–9.
4 Y. Wen, E. Gao, Z. Hu, T. Xu, H. Lu, Z. Xu and C. Li, *Nat. Commun.*, 2019, **10**, 2446.
5 P. Kot, J. Parnell, S. Habibian, C. Straßer, P. M. Ostrovsky and C. R. Ast, *Phys. Rev. B*, 2020, **101**, 235116.
6 S. K. Achar, L. Zhang and J. K. Johnson, *J. Phys. Chem. C*, 2021, **125**, 14874–14882.
7 A. Kouloumpis, D. D. Chronopoulos, G. Potsi, M. Pykal, J. Vlček, M. Scheibe and M. Otyepka, *Chem.–Eur. J.*, 2020, **26**, 6518–6524.
8 R. A. Schäfer, J. M. Englert, P. Wehrfritz, W. Bauer, F. Hauke, T. Seyller and A. Hirsch, *Angew. Chem., Int. Ed.*, 2013, **52**, 754–757.
9 A. Y. S. Eng, H. L. Poh, F. Šaněk, M. Maryško, S. Matějková, Z. Sofer and M. Pumera, *ACS Nano*, 2013, **7**, 5930–5939.
10 A. Y. Eng, Z. Sofer, P. Šimek, J. Kosina and M. Pumera, *Chem.–Eur. J.*, 2013, **19**, 15583–15592.
11 J. Sofo, A. Chaudhari and G. Barber, *Phys. Rev. B: Condens. Matter Mater. Phys.*, 2006, **75**, 153401.
12 F. Karlický, K. Kumara Ramanatha Datta, M. Otyepka and R. Zbořil, *ACS Nano*, 2013, **7**, 6434–6464.
13 R. R. Nair, W. Ren, R. Jalil, I. Riaz, V. G. Kravets, L. Britnell, P. Blake, F. Schedin, A. S. Mayorov, S. Yuan, M. I. Katsnelson, H. M. Cheng, W. Strupinski, L. G. Bulusheva, A. V. Okotrub, I. V. Grigorieva, A. N. Grigorenko, K. S. Novoselov and A. K. Geim, *Small*, 2010, **6**, 2877–2884.
14 S. Boopathi, T. Narayanan and S. SenthilKumar, *Nanoscale*, 2014, **6**, 10140–10146.
15 H. Poh, Z. Sofer, K. Szokolova and M. Pumera, *J. Mater. Chem. C*, 2014, **2**, 5198–5207.
16 R. Paupitz, P. A. S. Autreto, S. B. Legoas, S. G. Srinivasan, A. C. T. van Duin and D. S. Galvão, *Nanotechnology*, 2012, **24**, 035706.
17 T. Pandey, L. Covaci and F. M. Peeters, *Carbon*, 2021, **171**, 551–559.
18 R. Santosh and V. Kumar, *Solid State Sci.*, 2019, **94**, 70–76.
19 N.-C. Ri, J.-H. Wi, N.-H. Kim and S.-I. Ri, *Phys. E*, 2019, **108**, 226–232.
20 I. Papadakis, Z. Bouza, S. Couris, A. Bourlinos, V. Mouselimis, A. Kouloumpis, D. Gournis, A. Bakandritsos, J. Ugolotti and R. Zboril, *J. Phys. Chem. C*, 2017, **121**, 22567–22575.
21 U. Rajeena, M. Akbar, P. Raveendran and R. M. Ramakrishnan, *New J. Chem.*, 2018, **42**, 9658–9665.
22 B. B. Xiao, L. Yang, H. Y. Liu, X. B. Jiang, B. Aleksandr, E. H. Song and Q. Jiang, *Appl. Surf. Sci.*, 2021, **537**, 147846.

23 M. Ong, K. A. Duerloo and E. Reed, *J. Phys. Chem. C*, 2013, **117**, 3615–3620.
24 H. Kim, M. Noor-A-Alam, J. Son and Y.-H. Shin, *Chem. Phys. Lett.*, 2014, **603**, 62–66.
25 C. Q. Qu, C. Y. Wang, L. Qiao, S. S. Yu and H. B. Li, *Chem. Phys. Lett.*, 2013, **578**, 97–101.
26 D. B. Zhang and T. Dumitrică, *J. Chem. Phys.*, 2011, **134**, 196101.
27 I. I. Pronin, S. M. Dunaevskii, E. Y. Lobanova and E. K. Mikhailenko, *Phys. Solid State*, 2017, **59**, 2063–2069.
28 F. Zou, L. Zhu and K. Yao, *Sci. Rep.*, 2015, **5**, 1–10.
29 L. Cao, X. Li, Y. Li and G. Zhou, *J. Mater. Chem. C*, 2020, **8**, 9313–9321.
30 X.-Q. Cui, Q. Liu, Z.-Q. Fan and Z.-H. Zhang, *Org. Electron.*, 2020, **84**, 105808.
31 D. Zou, B. Cui, C. Fang, W. Zhao, C. Kong, D. Li, M. Zhao and D. Liu, *Org. Electron.*, 2015, **27**, 212–220.
32 G. Kresse and J. Furthmüller, *Phys. Rev. B: Condens. Matter Mater. Phys.*, 1996, **54**, 11169.
33 J. Perdew, K. Burke and M. Ernzerhof, *Phys. Rev. Lett.*, 1996, **77**, 3865–3868.
34 M. Brandbyge, J.-L. Mozos, P. Ordejón, J. Taylor and K. Stokbro, *Phys. Rev. B: Condens. Matter Mater. Phys.*, 2002, **65**, 165401.
35 J. Taylor, H. Guo and J. Wang, *Phys. Rev. B: Condens. Matter Mater. Phys.*, 2001, **63**, 245407.
36 P. Błoński, J. Tuček, Z. Sofer, V. Mazánek, M. Petr and M. Pumera, *J. Am. Chem. Soc.*, 2017, **139**, 3171–3180.
37 K. Saritas, C. Ataca and J. C. Grossman, *J. Phys. Chem. C*, 2015, **119**, 5074–5079.
38 J. Huang, L. Valenzano, T. V. Singh, R. Pandey and G. Sant, *Cryst. Growth Des.*, 2014, **14**, 2158–2171.
39 X. L. Wang, *Phys. Rev. Lett.*, 2008, **100**, 156404.
40 G. Y. Gao and K.-L. Yao, *Appl. Phys. Lett.*, 2013, **103**, 232409.
41 G. Y. Gao, G. Ding, J. Li, K.-L. Yao, M. Wu and M. Qian, *Nanoscale*, 2016, **8**, 8986.
42 Z. Jiang, H. Wang, Y. Wang, S. Sanvito and S. Hou, *J. Phys. Chem. C*, 2017, **121**, 27344–27350.